

Interaction of a Low-Power Laser Radiation with Nanoparticles Formed over the Copper Melt in Rarefied Argon Atmosphere

Leonid A. Dombrovsky^{1,2,*}  and Vladimir Ya. Mendeleyev³

¹ Heat Transfer Laboratory, Joint Institute for High Temperatures, 17A Krasnokazarmennaya St, 111116 Moscow, Russia

² X-BIO Institute, University of Tyumen, 6 Volodarskogo St, 625003 Tyumen, Russia

³ Laboratory of Physical Modelling of Two-Phase Flows, Joint Institute for High Temperatures, 13 (Bd 2) Izhorskaya St, 125412 Moscow, Russia; v_mendeleyev@list.ru

* Correspondence: ldomb@yandex.ru

Abstract: Two effects have been recently observed by the authors for the copper sample melted in a rarefied argon atmosphere. The first of these effects is a strong decrease in the normal reflectance of a copper sample with time just after the beginning of melting. A partially regular crystal structure was also formed on the surface of the solid sample after the experiment. Both effects were explained by generation of a cloud of levitating nanoparticles. Additional experiments reported in the present paper show that the rate of decrease in reflectance increases with pressure of argon atmosphere and the surface pattern on the solid sample after the experiment depends on the probe laser radiation. It is theoretically shown for the first time that the dependent scattering effects in the cloud of copper nanoparticles are responsible for the abnormal decrease in normal reflectance and also for the observed significant role of light pressure in deposition of nanoparticles on the sample surface. The predicted minimum of normal reflectance is in good agreement with the experimental value.

Keywords: copper melt; vapor condensation; levitating nanoparticles; rarefied argon atmosphere; Rayleigh scattering; normal reflectance; dependent scattering; deposition of particles; light pressure



Citation: Dombrovsky, L.A.; Mendeleyev, V.Y. Interaction of a Low-Power Laser Radiation with Nanoparticles Formed over the Copper Melt in Rarefied Argon Atmosphere. *Thermo* **2021**, *1*, 1–14. <https://dx.doi.org/10.3390/thermo1010001>

Received: 12 November 2020

Accepted: 8 December 2020

Published: 16 December 2020

Publisher's Note: MDPI stays neutral with regard to jurisdictional claims in published maps and institutional affiliations.



Copyright: © 2020 by the authors. Licensee MDPI, Basel, Switzerland. This article is an open access article distributed under the terms and conditions of the Creative Commons Attribution (CC BY) license (<https://creativecommons.org/licenses/by/4.0/>).

1. Introduction

The experimental and theoretical study presented here was started in connection with the traditional task of determining the change in spectral optical properties of chemically pure copper during its melting. Laboratory experiments in a vacuum chamber at a very low pressure of argon showed that the specular reflection of the probe laser radiation from the copper sample strongly decreases, almost immediately after the beginning of copper melting. To the best of our knowledge, this effect was observed and published in Reference [1] for the first time. The qualitative explanation of the observation, proposed by the authors, was associated with the condensation of copper vapor with formation of sub-micron particles of the melt above the sample surface. A qualitative analogy with the formation of the so-called droplet cluster levitating over a locally heated water surface [2,3] was used. This assumption was supported by the calculations based on the published data for mass flow rate of copper vapor in vacuum at temperatures greater than the melting point. A preliminary explanation of the decrease in normal reflectance of the copper sample in Reference [1] was based on the Mie scattering of light by small copper particles. The hypothesis of formation of a cloud of such particles was also supported by specific patterns with numerous small crystals of copper on the surface of the solid sample after the experiments.

The production of metal nanoparticles by vapor condensation has more than twenty years of history and, along with other methods of nanoparticle production, uses continuously developing advanced technologies [4–17]. Of course, the methods used in the industrial production of metal nanoparticles differ significantly from the electrical heating

of a metal sample in our laboratory study. At the same time, the effect of surrounding inert gas on the formation of nanoparticles and their clusters, as well as the features of the optical and mechanical interaction of laser radiation with nanoparticles, are still of theoretical interest. The authors believe that understanding physical processes under consideration may also be useful in some engineering or biomedical applications.

In contrast to Reference [1], a physically more sophisticated model for the effect of a cloud of copper nanoparticles on a strong decrease in the reflection of probe laser radiation is developed in the present paper. Special attention is also paid to the deposition of particles on the sample surface at the end of the experiment. The experimentally observed significant light-pressure effect on the deposition of copper nanoparticles on the sample surface is explained for the first time. The dependent scattering of closely spaced particles is a physical basis of the model developed.

2. Laboratory Set-Up and Experimental Procedure

The laboratory set-up is schematically presented in Figure 1. The bead of a high-temperature thermocouple was separated from the lower surface of the sample by a 100 μm layer of nickel. The melting temperature of nickel is about 400 K higher than that of copper, and the sufficiently high thermal conductivity of nickel makes it possible to consider the measured temperature close to the temperature of the copper sample. The probe laser with wavelength of $\lambda = 660 \text{ nm}$, power of $P = 40 \text{ mW}$, and average beam radius of $r = 3 \text{ mm}$ was used. The incidence angle was about 5° . The fluctuations of laser power were measured by sensor 11, whereas sensor 12 was used to measure the radiative power reflected from the sample in the specular direction. The corresponding relative value is hereafter referred to as the normal reflectance.

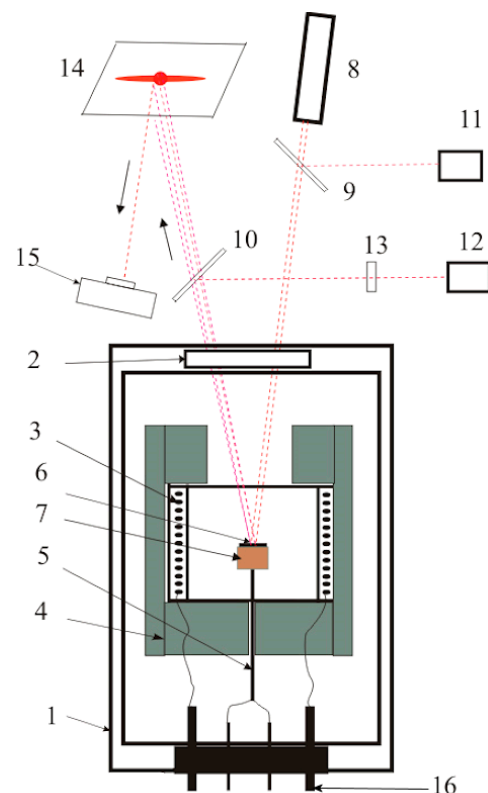


Figure 1. The schematic of the laboratory set-up: 1—vacuum chamber, 2—optical window, 3—electric heater, 4—thermal insulation, 5—thermocouple, 6—copper sample, 7—nickel substrate, 8—probe laser, 9 and 10—semi-transparent mirrors, 11 and 12—sensors, 13—interference filter, 14—flat screen, 15—digital camcorder, and 16—electrical connector. Reprinted with permission from Reference [1]. Copyright 2020 Elsevier.

Both the screen and camcorder were used to observe the patterns of the light scattered by the sample. The thermo-emf of thermocouple, the data of sensors, and the scattering patterns were registered by a computer with time interval of 1 s. Note that the error of the normal reflectance measurements is explained mainly by fluctuations of the laser radiation flux. The measured relative value of these fluctuations is from 0.13% to 0.2%.

The sample of 99.9% Cu (according to the local manufacturer's certificate) was placed in a vacuum chamber filled by argon at pressure of $p = 10$ kPa or $p = 30$ kPa. The upper surface of a cylindrical copper sample of diameter 10 mm and height of $H = 2.2$ mm was ground in one direction. The grooves of roughness of about 70 nm on the original surface make evident the melting of a surface layer with the use of scattering patterns. At low temperatures, the pattern looks like a bright central spot and the narrow strip in the direction perpendicular to the grooves. Obviously, the melt surface is smooth, and the copper melting can be well identified by disappearing the strip. This technique, proposed in Reference [18], was also successfully used by the authors in Reference [1].

The position of the thermocouple is schematically presented in Figure 2, where r is the radial coordinate measured from the axis of the thermocouple. The difference between the temperature of the upper surface of the copper sample, T , and the measured temperature of the thermocouple bed, T_m , can be estimated as follows:

$$\Delta T = T - T_m = \varepsilon \sigma T^4 H / k_c, \quad (1)$$

where ε is the integral emissivity of the sample surface, σ is the Stefan–Boltzmann constant, and k_c is the thermal conductivity of copper. Let us consider the most interesting case of $T = 1358$ K (the melting temperature of copper). With the use of an average value of $\varepsilon = 0.5$ (taking into account a partial shielding of thermal radiation by a cloud of nanoparticles, see below) and $k_c = 175$ W/(m K) (for liquid copper), we obtain $\Delta T \approx 1.2$ K. This temperature difference is sufficiently small to be neglected in further analysis.

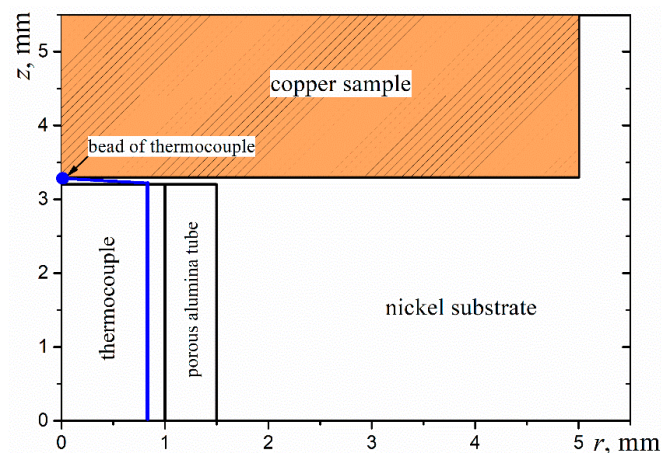


Figure 2. Schematic of the thermocouple design and position.

3. The Decrease in Reflectance of Molten Copper

Typical time variation of the thermo-emf of thermocouple, U , which is directly proportional to the sample temperature, and the relative normal reflectance of the copper sample, $R_n = R_n / R_n^{\max}$ ($R_n^{\max} \approx 0.84$ is the maximum normal reflectance in the beginning of melting), are presented in Figure 3. The horizontal “plateau” in the dependence of $U(t)$ in Figure 3a is explained by the latent heat of copper melting. One can see that the melting time of the sample depends on the argon pressure. This is explained by shielding thermal radiation from the melt surface by the cloud of copper nanoparticles. The cloud of particles is formed faster in the case of higher pressure of argon due to the larger number of condensation nuclei. As a result, the time of melting at $p = 30$ kPa is several times less than that at $p = 10$ kPa. This is another confirmation of the existence of a cloud of copper

nanoparticles, which absorbs both visible laser radiation and infrared radiation from the sample of molten copper.

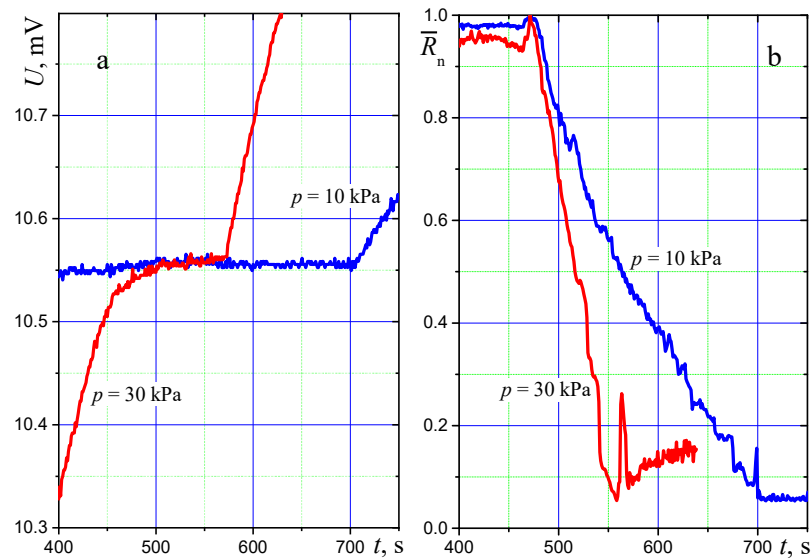


Figure 3. Time variation of (a) thermo-emf of thermocouple and (b) relative normal reflectance in the experiments with different pressures of argon.

One can see in Figure 3b that the normal reflectance of molten copper sample decreases strongly with time. The experiments showed that the rate of the reflectance decrease is greater in the case of a relatively large pressure of argon in the vacuum chamber. The results obtained for the effect of argon pressure agree well with the data of Reference [19] on the important role of argon atmosphere in the formation of condensation nuclei. Note that the minimum value of relative reflectance observed at the final stage of copper melting is equal to $R_n^{\min} \approx 0.04$ for both values of argon pressure. It means that the probe laser beam does not reach the surface of the copper sample because the optically thick particle cloud totally attenuates the probe laser beam at this period.

At the beginning of melting, the laser light is reflected from the absolutely smooth surface of copper melt (the normal reflectance R_n^{\max} is very large), and after a while (the less the higher argon pressure), the reflectance becomes extremely weak. The same value of R_n^{\min} at various values of the argon pressure indicates that we are dealing with a very remarkable situation when the optical properties of a cloud of copper nanoparticles levitating above the sample surface are weakly sensitive to the conditions of the particle cloud formation. The latter circumstance suggests a physical assumption that the nanoparticles satisfy the conditions of the Rayleigh theory, when the radiation extinction does not depend on the particle size distribution and the extinction value is determined only by the volume fraction of particles and the cloud thickness. With a large optical thickness of the cloud of nanoparticles, their volume fraction also ceases to be a parameter of the problem. As will be shown in the theoretical part of the paper, it is under such conditions that the value of R_n^{\min} is determined only by the spectral optical constants of copper at the wavelength of laser radiation.

It should also be noted that the diameter of the bright spot on the screen increases slightly during a strong decrease of the normal reflectance (only 20% during the melting period). The increase in the corresponding scattering angle is a secondary effect that is not considered in the developed model.

4. Surface Patterns on Samples of Solid Copper Samples after the Experiments

The photograph of the surface of the solid sample before the experiment with the mentioned grooves is presented in Figure 4a. The grooves disappear just after the melting of copper and the surface of the molten sample becomes perfectly smooth. However, the

images of the sample surface after the experiment (Figure 4b–d) show that the surface is covered by small crystals.

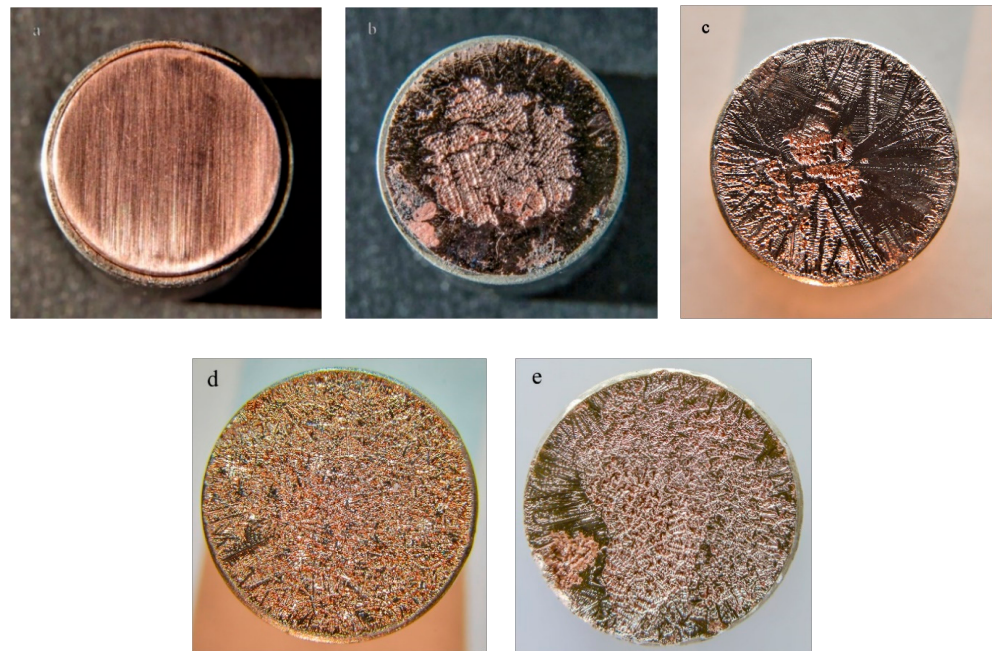


Figure 4. Photographs of the surface of solid copper samples (a) before the experiments and (b–e) after the experiments: (b,c)— $p = 10$ kPa, (d,e)— $p = 30$ kPa, (b,d)—the probe laser was on, (c,e)—the probe laser was off during the experiment.

Most likely, these crystals are formed due to the deposition and subsequent growth of copper particles [5,20,21]. It is interesting that the surface pattern depends considerably on the probe laser radiation. In fact, the same experiments with the turned off laser yield the other surface patterns (Figure 4c,e). The evident effect of a low-power laser radiation on the surface pattern (compare Figure 4b,d and Figure 4c,e) is one of the main motivations of the physical modeling considered below. Note that heating of the sample in the experiment with the turned-off probe laser was almost the same as that in the main experiment (Figure 5). In other words, the laser radiation does not affect the sample heating. This experimental result is consistent with the obvious estimate, since the power of the probe laser is much lower than the power of the electric heater.

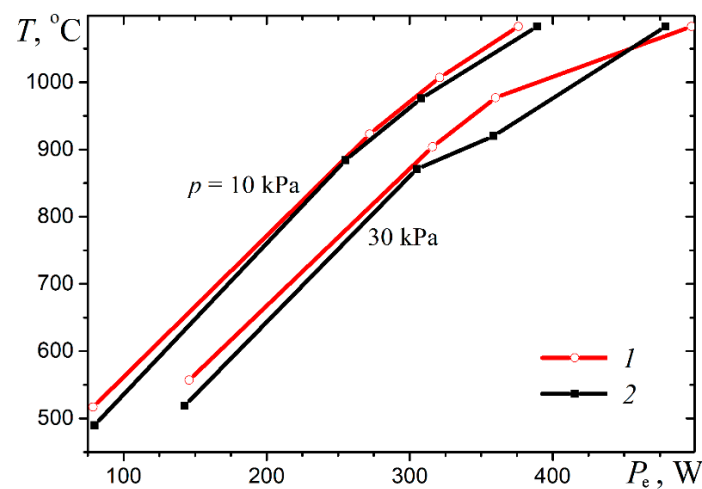


Figure 5. Temperature of the copper sample as a function of electric power in the experiments with different values of argon pressure when the probe laser is (1) turned on or (2) turned off during the experiment.

5. Theoretical Model for Interaction of Laser Radiation with a Cloud of Copper Nanoparticles

As described in the experimental part of the paper, two main physical effects of interaction of the probe laser radiation with copper nanoparticles condensed from the copper vapor above the melt surface are observed. First, the growing cloud of nanoparticles leads to a strong decrease in the normal reflectance of the laser beam. Secondly, the light of a probe laser considerably affects the rough structure of the surface of the solid sample after the experiment. Both observations should be taken into account in theoretical modeling.

5.1. Optical Properties of Single Nanoparticles of Copper

It is natural to begin from the calculations of interaction of the incident light by a single spherical particle. This is described by the Mie theory [22–26] and depends on two parameters: the diffraction parameter $x = 2\pi a / \lambda$ (a is the particle radius) and the complex index of refraction, $m = n - i\kappa$, where n and κ are the spectral indices of refraction and absorption. We will consider the following resulting values of Mie calculations performed using the computer code from early book [27]: Q_a , Q_s^{tr} , and $Q_{\text{tr}} = Q_a + Q_s^{\text{tr}}$, which are the efficiency factor of absorption, the transport efficiency factor of scattering, and the transport efficiency factor of extinction, respectively. It should be recalled that with the use of transport approximation, the scattering phase function in the radiative transfer equation [28–30] is replaced by a sum of the isotropic component and the term describing the peak of forward scattering [28,31,32]. This approach is widely used, and it is usually rather accurate in solving the radiative transfer problems characterized by multiple scattering when the details of angular pattern of single scattering are not important. However, for the particular problem under investigation, it is also interesting to consider the scattering phase function for the randomly polarized radiation, $g(\theta)$, where θ is the angle of scattering.

The spectral optical constants of copper have been studied in detail for solid copper [33,34]. Note that the measurements reported in References [35–37] showed a considerable increase in normal emittance of copper at the melting, but there is no detailed spectral data for optical properties of molten copper in the visible range [38]. Therefore, we used a linear interpolation of tabulated optical constants of solid copper reported in Reference [33] with the resulting values of indices of refraction and absorption $n = 0.128$ and $\kappa = 3.754$ at $\lambda = 660$ nm.

Some results of calculations using the rigorous Mie theory and the Rayleigh theory (when scattering is symmetric and $Q_s^{\text{tr}} = Q_s$) [28] are presented in Figure 6. One can see in Figure 6a, that the absorption of radiation by copper particles is much less than scattering and the maximum value of $Q_{\text{tr}} \approx 4$ is reached at $a = 96$ nm. The predominant scattering (as compared to absorption) is not typical of the Rayleigh particles. The result obtained for copper nanoparticles is explained by a very low index of refraction of copper in the visible spectral range [28]. It is interesting that simple equations of the Rayleigh theory give rather accurate results for Q_{tr} when $a < 100$ nm. In this interval of particle radii, $g(\theta)$ is also close to that for the Rayleigh scattering, whereas the larger particles are characterized by a predominant forward scattering (Figure 6b). In further analysis, we will assume that copper nanoparticles are sufficiently small to satisfy the conditions of the Rayleigh theory.

It should be noted that there is a principal difference between the copper nanoparticles under consideration and plasmonic nanoparticles widely used in biomedicine and many other applications [39–42]. The Mie calculations do not show the plasmonic resonances of absorption for single copper nanoparticles in the visible spectral range. At the same time, it was found in Reference [43] that regular hexagonal structures of copper particles of size 20–40 nm with a “period” of 390 nm exhibit the plasmonic behavior and absorption peaks in the visible range. Of course, we have no information about possible regular structures in the cloud of particles above the sample of molten copper. However, one cannot exclude that similar structures can be formed time by time in the particle cloud.

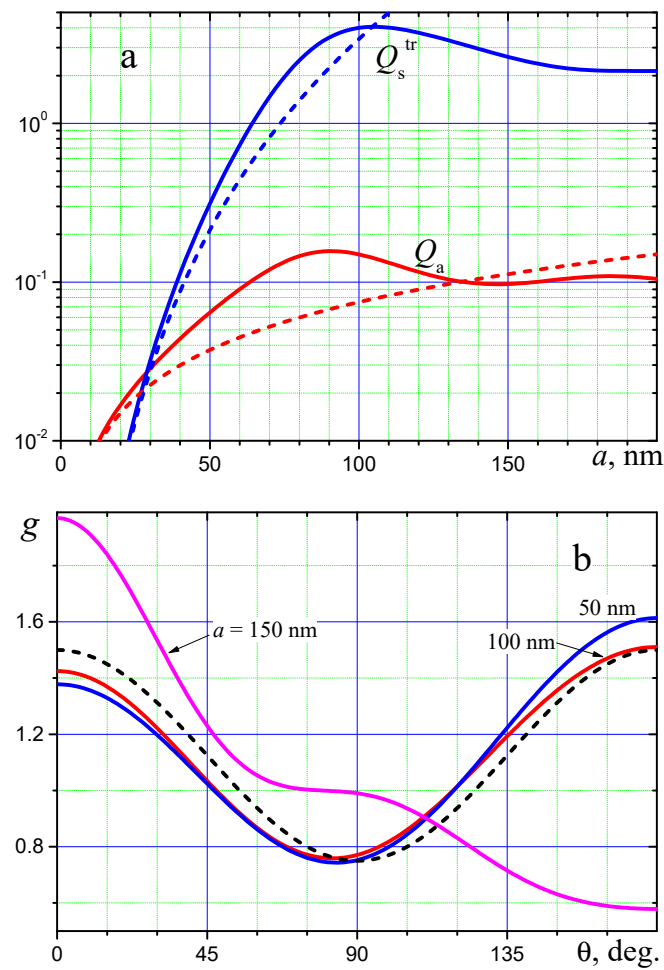


Figure 6. Optical properties of spherical copper particles at wavelength $\lambda = 660$ nm: (a)—the efficiency factor of absorption and transport efficiency factor of scattering, (b)—the scattering phase function of single scattering. Solid lines—the Mie theory, dashed lines—the Rayleigh theory. The angle of scattering is measured from the direction of incident light.

5.2. Light Pressure of Probe Laser Beam on a Copper Nanoparticle

The force of light pressure of laboratory laser beam on a single spherical particle of copper can be calculated as follows [22]:

$$F_{\text{rad}} = \pi a^2 Q_{\text{tr}} q / c_0, \quad (2)$$

where $q = P / (\pi r^2) \approx 1.4 \text{ kW/m}^2$ is the average incident radiative flux and $c_0 = 3 \times 10^8 \text{ m/s}$ is the speed of light. As the above calculations for single particles in Section 5.1, Equation (2) can be used only in the case of the so-called independent scattering when each particle absorbs and scatters the light in exactly the same manner as if other particles do not exist. In addition, this approach is applicable when there is no systematic phase relation between partial waves scattered by individual particles during the observation time interval, so that the intensities of the partial waves can be added without regard to phase. In the case of independent scattering, each particle is in the far-field zones of all other particles and scattering by individual particles is incoherent. The hypothesis of independent scattering is usually true when the distance between randomly positioned particles is greater than both the particle size and the wavelength [44–49]. It is highly likely that the last of these conditions is not satisfied during the main part of the melting period of copper samples.

Note that even with independent scattering, even a particle not shaded by other particles is illuminated not only directly by laser, but also by the light scattered by other particles

of a cloud. Moreover, with a small optical thickness of the particle cloud, one should take into account the light reflected from the surface of the copper sample. This means that the complete solution to the problem should include the calculation of radiative transfer in a cloud of particles, as was done, for example, in Reference [50]. At the same time, the upper estimate of the light pressure force on an “independent” particle located near the illuminated surface of the cloud can be made using Equation (2).

It is convenient to consider the force of light pressure related to the particle weight:

$$F_{\text{rad}} = \frac{F_{\text{rad}}}{mg} = 0.75 \frac{Q_{\text{tr}}}{\alpha} \frac{q}{\rho g c_0}, \quad (3)$$

where $\rho = 8000 \text{ kg/m}^3$ is the density of copper melt, and $g = 9.81 \text{ m/s}^2$ is the acceleration of gravity. The Mie theory calculations show the maximum value of the ratio of $Q_{\text{tr}}/a = 41.8 \text{ } \mu\text{m}^{-1}$ at $a = 97 \text{ nm}$ (see Figure 7). The corresponding maximum value of F_{rad} is about 1.9×10^{-3} . This result is in obvious contradiction with the laboratory observations of the effect of laser light on deposition of particles on the sample surface. This is one more argument to take into account the effect of dependent scattering which is expected to be significant.

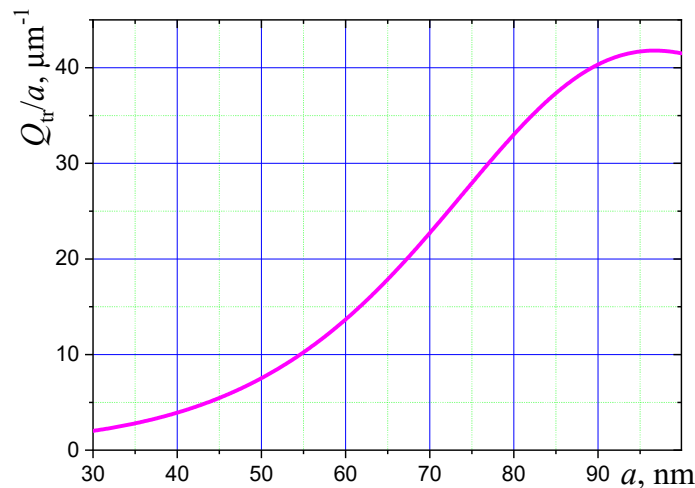


Figure 7. The calculated ratio of transport efficiency factor of extinction to the radius of copper particle at wavelength $\lambda = 660 \text{ nm}$.

5.3. The Model of Dependent Scattering and Explanation of the Observed Decrease in Reflectance

With the dependent scattering, the laser radiation does not act on a single nanoparticle, but on some clusters of a large number of closely spaced nanoparticles. This problem is physically similar to that for water droplets in the microwave (radar) remote sensing of highly turbulent cumulus clouds in the atmosphere when the radiation wavelength is much greater than both the droplet size and the distances between the neighboring droplets [51]. However, in contrast to atmospheric clouds, the cloud of copper nanoparticles is not isotropic. It is expected that this cloud is almost flat like the droplet cluster over the locally heated water surface [52,53], but particles of copper are not regularly positioned and can form a multilayer optically thick structure.

The main assumption of the suggested theoretical model of reflection of laser radiation from a cloud of copper nanoparticles is that the optical properties of individual nanoparticles, which are considered spherical, are well described by the Rayleigh theory. The above calculations based on the Mie theory showed that at the wavelength $\lambda = 660 \text{ nm}$, this assumption is valid even for rather large copper particles, which satisfy the condition of $a < 100 \text{ nm}$. In other words, the spectral optical properties of copper nanoparticles can be calculated using the dipole approximation. As a result, the effective optical properties of a conventionally uniform cloud of particles can be easily determined.

To estimate the effective optical constants of a cloud of spherical copper nanoparticles, we assume that at each time moment, the nanoparticles have the same size and are uniformly distributed over the volume of a plane-parallel layer. Note that the assumption of monodisperse nanoparticles is not important in the Rayleigh theory. With a large number of Rayleigh particles, the Maxwell-Garnett theory can be used to determine the optical constants of a homogeneous layer [54,55]. This approach is widely used in quite different applications including the recent paper, Reference [56], for nanoparticles of soot in ice grains of the polluted snow. The complex permittivity of a cloud medium is calculated in terms of particle polarizability by applying the Lorentz–Lorenz formula [57,58]. In our case, there is no refractive and absorbing host medium and the effective complex index of refraction, $m_{\text{eff}} = n_{\text{eff}} - ik_{\text{eff}}$, is expressed relatively simple:

$$m_{\text{eff}}^2 = \frac{1 + 2f_v\psi}{1 - f_v\psi}, \quad \psi = \frac{m^2 - 1}{m^2 + 2}, \quad (4)$$

where f_v is the volume fraction of particles in the cloud. Having substituted the value of $m = 0.128 - 3.754i$ to the second of Equation (4), we obtain:

$$\psi = 1.247 - 0.0196i. \quad (5)$$

The observed minimum value of normal reflectance, $R_n^{\text{min}} = R_n^{\text{min}} \times R_n^{\text{max}} \approx 0.04 \times 0.84 = 0.336$, at the final stage of melting of the copper sample (Figure 3b) indicates that the optical thickness of a cloud of copper nanoparticles over the sample surface is sufficiently large ($\tau > 1$). On the other hand, the known equation can be used for the normal reflectance of the optically thick cloud when $\kappa_{\text{eff}} \ll n_{\text{eff}}$ (we will see that this condition is satisfied) is as follows:

$$R_n^{\text{min}} = \left(\frac{n_{\text{eff}} - 1}{n_{\text{eff}} + 1} \right)^2, \quad (6)$$

and one can easily obtain $n_{\text{eff}} = 1.45$. Substituting this value to the first of Equation (4) yields $f_v \approx 0.22$ and $\kappa_{\text{eff}} = 8.2 \times 10^{-3} \ll n_{\text{eff}}$. It is interesting that the calculated volume fraction of copper nanoparticles in the cloud in a combination with any realistic cloud thickness explains the decrease in the normal reflectance observed in the laboratory experiments. In other words, the generated particle cloud with a thickness of a few micrometers is sufficient to explain the observed value of $R_n^{\text{min}} \approx 0.04$, which does not depend on the particle size.

The spectral absorption coefficient of the cloud of copper nanoparticles is [59]:

$$\alpha_{\text{eff}} = 4\pi\kappa_{\text{eff}}/\lambda \approx 0.156 \mu\text{m}^{-1} \quad (7)$$

and the dimensionless optical thickness, τ , of the cloud of geometrical thickness, d , is equal to $\tau = \alpha_{\text{eff}}d$. In the particular case under consideration, the condition of $\tau > 1$ yields the following estimation for the cloud thickness:

$$d > 6.4 \mu\text{m}. \quad (8)$$

The measured time variation of the normal reflectance of the molten copper sample (Figure 3b) in the range from the maximum to the minimum value is almost monotonic and can be well approximated by the following function:

$$R_n(t) = R_n^{\text{min}} + (1 - R_n^{\text{min}}) \exp\left(-\left(\frac{t - t_0}{t_*}\right)^\gamma\right), \quad \gamma = 1 + \zeta(t - t_0)/t_*, \quad (9)$$

where t_* is the characteristic time for the initial period of copper evaporation when the optical thickness of the nanoparticle cloud increases linearly with time (following the constant evaporation rate). Equation (9) takes into account an almost linear increase in

the optical thickness of the nanoparticle cloud (τ_{eff}) with time just after the beginning of melting (due to the constant flow rate of copper evaporation), and also the faster increase in τ_{eff} up to the minimum reflectance when the number of levitating copper nanoparticles becomes rather large. The values of $t_* = 120$ s and $\zeta = 0.3$ give good approximation of the experimental data obtained at $p = 10$ kPa, whereas the values of $t_* = 53$ s and $\zeta = 0.9$ are appropriate in the case of 30 kPa pressure of argon. The resulting approximations are shown in Figure 8.

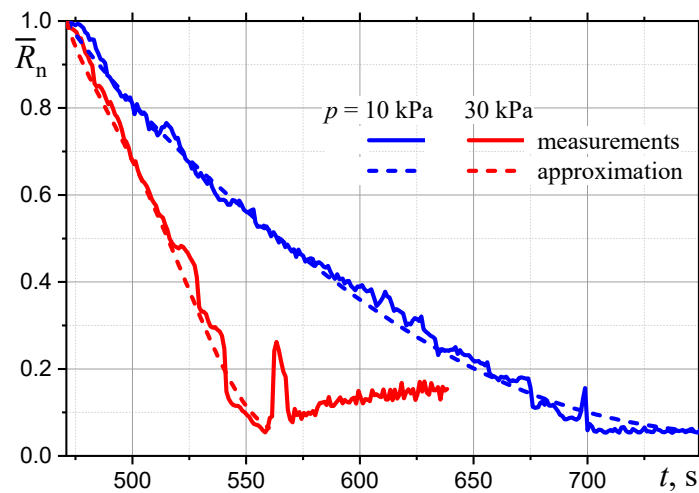


Figure 8. Time dependences of the normal reflectance of the molten copper sample.

The monotonic decrease in the normal reflectance of the sample (see Equation (9)), corresponds to the formation of an optically thick cloud of copper nanoparticles above the sample. This process continues throughout the copper melting time. Heating of the sample continues after melting is complete, when the copper temperature rises rapidly (Figure 3a), and the experiments show more complex changes in reflectance with time (Figures 3b and 8). First of all, it is interesting that there is a strong peak of reflectance just after the end of the copper melting. Most likely, this peak observed at different pressures of argon is explained by the fast increase in the melt temperature shown in Figure 3a. A rapid increase in the rate of evaporation of copper with an increase in the melt temperature leads to the fact that the upward flow of copper vapor partially destroys the cloud of nanoparticles. In this case, the effective optical thickness of the cloud temporarily decreases. Note that this effect is very similar to a short-term increase in the intensity of water evaporation, which was used in Reference [60] to form the droplet clusters containing the given small number of almost identical large water droplets. In our case, the subsequent formation of new nanoparticles of copper leads to the restoration of an almost opaque layer of these particles.

The second special feature of the experimental dependence of $R_n(t)$ at $p = 30$ kPa is an increase in the reflectance just after the peak (Figure 8). This is explained by the increase in the melt temperature (Figure 3a), which apparently leads to an increase in volume fraction of nanoparticles and the resulting increase in the reflectance. The calculations for the value of $R_n = 0.16$ observed at $t = 640$ s yield $n_{\text{eff}} = 2.16$ and $\kappa_{\text{eff}} = 0.03$. Note that the corresponding high value of $f_v \approx 0.44$ indicates that copper nanoparticles are polydisperse. The calculated value of f_v confirms that there is an increase in the volume fraction of copper nanoparticles above the sample in the period of $570 < t < 640$ s in the experiment with 30 kPa argon pressure.

5.4. Possible Explanation of Considerable Contribution of Light Pressure to the Deposition of Particles

Let us estimate the light pressure from the probe laser beam on the cloud of nanoparticles for the conditions of the laboratory experiments. Of course, the pressure of light on the particles located in the lower part of the optically thick cloud is insignificant, since the

laser light is almost completely absorbed by the nanoparticles located above, closer to the illuminated surface of the particle cloud. Therefore, it is interesting to evaluate the force of light pressure on the upper layer of nanoparticles.

When calculating the reflectance of a cloud of copper nanoparticles, it was sufficient to use the monodisperse approximation. On the contrary, when determining the force of light pressure on the upper layer of particles, it should be taken into account that the size of nanoparticles in this layer is apparently much smaller than the average size of particles in the cloud. The latter is explained by a decrease in the local flow rate of copper vapor with the distance from the melt surface.

Of course, it would be incorrect to consider the pressure of light on single copper nanoparticles, ignoring the significant effect of dependent scattering. For estimation, we will assume that laser radiation is almost completely absorbed in the surface monolayer of closely spaced identical spherical nanoparticles with radius a_{\min} . In this case, the ratio of the light pressure force to the total weight of nanoparticles in the upper layer is as follows:

$$F_{\text{rad}} = \frac{q}{2f_v a_{\min} \rho g c_0}. \quad (10)$$

It is assumed here that the monolayer thickness is equal to $2a_{\min}$. It is also natural to assume that volume fraction of nanoparticles in the upper layer is much smaller than the average value. The use of $f_v = 0.01$ and $a_{\min} = 5$ nm in Equation (10) yields the value of $F_{\text{rad}} = 0.59$. This result means that the radiation pressure of the probe laser can rather strongly influence the upper layer of copper nanoparticles. These relatively small particles move downward, colliding and probably coagulating with larger particles, which also begin to move towards the sample surface. The emerging “avalanche” of nanoparticles is apparently the physical reason for the effect of low-power laser radiation on the deposition of particles and the experimentally observed change in the surface structure of a solidifying copper sample.

6. Conclusions

It was shown that both the strong decrease in the normal reflectance of a molten copper sample in a rarefied argon atmosphere and the formation of a specific pattern on the surface of a solid sample after the experiment can be explained by generation of a cloud of nanoparticles of copper levitating above the sample. A decrease in the melting time of the sample with increasing argon pressure is also explained by the presence of a cloud of nanoparticles, which reduces the heat losses by shielding the thermal radiation of the copper sample.

The applicability of the Rayleigh theory for optical properties of single spherical nanoparticles of copper with radius less than 100 nm was confirmed by comparison with rigorous Mie theory calculations. A combination of the Rayleigh theory for single particles of copper and the Maxwell-Garnett theory for the particle cloud enabled us to obtain the minimum reflectance value, which is in good agreement with the laboratory measurements. Moreover, the developed model yielded realistic approximate values for the volume fraction of copper nanoparticles in the cloud.

As can be expected, the rate of condensation of nanoparticles from the copper vapor increased with the argon pressure in ambient rarefied atmosphere. At the same time, the argon pressure did not affect the minimum reflectance observed in the experiments. The latter was explained by the suggested theoretical model as a transfer to the limit of optically thick cloud containing the Rayleigh particles. The predicted minimum normal reflectance is in good agreement with the value determined experimentally.

The special features of experimental time dependences of the sample reflectance at the end of melting and also in the period of subsequent heating of copper melt were also physically explained in terms of the developed model. The observed narrow peak in the reflectance just after the end of melting was explained by the fast increase in the melt temperature. The resulting rapid increase in the rate of evaporation of copper led

to a partial destruction of the cloud of nanoparticles. The subsequent formation of new nanoparticles of copper led to the restoration of an almost opaque layer of these particles. A possible further increase in the reflectance is a result of an increase in the volume fraction of particles with the copper melt temperature.

It was experimentally proven that the force of light pressure from the probe laser beam on the cloud of copper nanoparticles significantly contributes to formation of a specific pattern on the surface of the solid copper sample after the experiment. The calculations based on the developed physical model confirmed that the force of light pressure on the upper layer of relatively small nanoparticles is comparable with the total weight of particles in this layer. These particles move downward, colliding and coagulating with larger particles, which also begin to move towards the sample surface. According to the model, the laser-induced “avalanche” of nanoparticles is a physical reason for the observed effect of laser radiation on the deposition of particles and the resulting change in surface structure of a solidifying copper sample. This can be treated as a qualitative validation of the theoretical model.

The suggested model for optical and mechanical interaction of a low-power laser beam and the cloud of levitating nanoparticles generated over the surface of molten metal in a rarefied medium of inert gas is expected to be useful in the work with the condensed metal nanoparticles in engineering applications.

Author Contributions: Conceptualization, theoretical analysis, calculations, and writing the paper—L.A.D.; design of the experimental set-up and experimental study—V.Y.M. Both authors have read and agreed to the published version of the manuscript.

Funding: This research was funded by the Russian Foundation for Basic Research, grant No. 19-08-00238a.

Acknowledgments: The authors are grateful to the Russian Foundation for Basic Research (project 19-08-00238a) for the financial support of the present study. We would also like to thank Vladimir V. Pilipenko for his kind assistance in the work with the experimental set-up.

Conflicts of Interest: The authors declare no conflict of interest.

References

1. Mendeleyev, V.Y.; Kachalov, V.V.; Kurilovich, A.V.; Dombrovsky, L.A. Abnormally strong decrease in reflectance of molten copper due to possible generation of levitating sub-micron melt droplets. *Int. J. Heat Mass Transf.* **2017**, *113*, 53–58. [[CrossRef](#)]
2. Fedorets, A.A. Droplet cluster. *JETP Lett.* **2004**, *79*, 372–374. [[CrossRef](#)]
3. Fedorets, A.A.; Dombrovsky, L.A. Self-assembled stable clusters of droplets over the locally heated water surface: Milestones of the laboratory study and potential biochemical applications. In Proceedings of the 16th International Heat Transfer Conference, Beijing, China, 10–15 August 2018. Keynote Lecture KN02.
4. Kruis, F.E.; Fissan, H.; Peled, A. Synthesis of nanoparticles in the gas phase for electronic, optical and magnetic application—A review. *J. Aerosol Sci.* **1998**, *29*, 511–535. [[CrossRef](#)]
5. Wegner, K.; Walker, B.; Tsantilis, S.; Pratsinis, S.E. Design of metal nanoparticle synthesis by vapor flow condensation. *Chem. Eng. Sci.* **2002**, *57*, 1753–1762. [[CrossRef](#)]
6. Swihart, M.T. Vapor-phase synthesis of nanoparticles. *Curr. Opin. Coll. Int. Sci.* **2003**, *8*, 127–133. [[CrossRef](#)]
7. Raffi, M.; Rumaiz, A.K.; Hasan, M.M.; Shah, S.I. Studies of growth parameters for silver nanoparticle synthesis by inert gas condensation. *J. Mater. Res.* **2007**, *22*, 3378–3384. [[CrossRef](#)]
8. Pérez-Tijerina, E.; Pinilla, M.G.; Mejía-Rosales, S.; Ortiz-Méndez, U.; Torres, A.; José-Yacamán, M. Highly size-controlled synthesis of Au/Pd nanoparticles by inert-gas condensation. *Faraday Discuss.* **2008**, *138*, 353–362. [[CrossRef](#)]
9. Gracia-Pinilla, M.; Martínez, E.; Vidaurri, G.S.; Pérez-Tijerina, E. Deposition of size-selected Cu nanoparticles by inert gas condensation. *Nanoscale Res. Lett.* **2010**, *5*, 180–188. [[CrossRef](#)]
10. Melendrez, M.F.; Vargas-Hernández, C. Growth and morphology of tin nanoparticles obtained by the condensation of metal vapors. *Rev. Mex. Fis.* **2013**, *59*, 39–45.
11. Maicu, M.; Schmittgens, R.; Hecker, D.; Glöss, D.; Gerlach, G. Synthesis and deposition of metal nanoparticles by gas condensation process. *J. Vac. Sci. Technol. A* **2014**, *32*, 02B113. [[CrossRef](#)]
12. Huttel, Y. (Ed.) *Gas-Phase Synthesis of Nanoparticles*; Wiley-VCH: Weinheim, Germany, 2017.
13. Bushan, B. (Ed.) *Springer Handbook of Nanotechnology*, 4th ed.; Springer: Berlin, Germany, 2017.
14. Deepak, F.L. (Ed.) *Metal Nanoparticles and Clusters. Advances in Synthesis, Properties and Applications*; Springer: Cham, Switzerland, 2018.
15. Thota, S.; Crans, D.C. (Eds.) *Metal Nanoparticles: Synthesis and Application in Pharmaceutical Sciences*; Wiley: New York, NY, USA, 2018.

16. Khandel, P.; Yadaw, R.K.; Deepack, K.S.; Kanwar, L.; Shahi, S.K. Biogenesis of metal nanoparticles and their pharmacological applications: Present status and application prospects. *J. Nanostruct. Chem.* **2018**, *8*, 217–254. [[CrossRef](#)]
17. Slepíčka, P.; Slepíčkova-Kasálková, N.; Siegel, J.; Kolská, Z.; Švorčík, V. Methods of gold and silver nanoparticles preparation. *Materials* **2020**, *13*, 1. [[CrossRef](#)] [[PubMed](#)]
18. Batenin, V.M.; Kachalov, V.V.; Kurilovich, A.V.; Mendeleyev, V.Y. Evolution of diffraction pattern of probing radiation reflected by a silver surface upon melting. *High Temp.* **2016**, *54*, 277–280. [[CrossRef](#)]
19. Khojasteh, M.; Kresin, V.V. Influence of source parameters on the growth of metal nanoparticles by sputter-gas-aggregation. *Appl. Nanosci.* **2017**, *7*, 875–883. [[CrossRef](#)]
20. Chepkasov, I.V.; Gafner, Y.Y.; Gafner, S.L.; Bardakhanov, S.P. The general mechanisms of Cu cluster formation in the process of condensation from the gas phase. *Bull. Mater. Sci.* **2015**, *38*, 701–706. [[CrossRef](#)]
21. Chepkasov, I.V.; Gafner, Y.Y.; Gafner, S.L. Changing in the shape and structure of Cu nanoclusters generated from a gas phase: MD simulations. *J. Aerosol Sci.* **2016**, *91*, 33–42. [[CrossRef](#)]
22. Van de Hulst, H.C. *Light Scattering by Small Particles*; Dover: New York, NY, USA, 1981.
23. Bohren, C.F.; Huffman, D.R. *Absorption and Scattering of Light by Small Particles*; Wiley: New York, NY, USA, 1998.
24. Mishchenko, M.I.; Travis, L.D.; Lacis, A.A. *Multiple Scattering of Light by Particles: Radiative Transfer and Coherent Backscattering*; Cambridge University Press: Cambridge, UK, 2006.
25. Hergert, W.; Wriedt, T. *The Mie Theory: Basics and Applications*; Springer: Berlin, Germany, 2012.
26. Gouesbet, G.; Gréhan, G. *Generalized Lorenz–Mie Theories, 2nd ed.*; Springer: Berlin, Germany, 2017.
27. Dombrovsky, L.A. *Radiation Heat Transfer in Disperse Systems*; Begell House: New York, NY, USA, 1996.
28. Dombrovsky, L.A.; Baillis, D. *Thermal Radiation in Disperse Systems: An Engineering Approach*; Begell House: New York, NY, USA, 2010.
29. Modest, M.F. *Radiative Heat Transfer*, 3rd ed.; Academic Press: New York, NY, USA, 2013.
30. Howell, J.R.; Mengüç, M.P.; Daun, K.; Siegel, R. *Thermal Radiation Heat Transfer*, 7th ed.; CRC Press: New York, NY, USA, 2020.
31. Dombrovsky, L.A. The use of transport approximation and diffusion-based models in radiative transfer calculations. *Comput. Therm. Sci.* **2012**, *4*, 297–315. [[CrossRef](#)]
32. Dombrovsky, L.A. Scattering of radiation and simple approaches to radiative transfer in thermal engineering and bio-medical applications. In *Springer Series in Light Scattering*; Kokhanovsky, A., Ed.; Springer: Darmstadt, Germany, 2019; Volume 4, pp. 71–127.
33. Schulz, L.G. The experimental study of the optical properties of metals and the relation of the results to the Drude free electron theory. *Adv. Phys.* **1957**, *6*, 102–144. [[CrossRef](#)]
34. Winter, J.; Rapp, S.; Schmidt, M.; Huber, H.P. Ultrafast laser processing of copper: A comparative study of experimental and simulated transient optical properties. *Appl. Surf. Sci.* **2017**, *417*, 2–15. [[CrossRef](#)]
35. Watanabe, H.; Susa, M.; Nagata, K. Discontinuity in normal spectral emissivity of solid and liquid copper at the melting point. *Metall. Mater. Trans.* **1997**, *28A*, 2507–2513. [[CrossRef](#)]
36. Peletskii, V.E. Investigation of the monochromatic emissivity of liquid copper. *High Temp.* **2000**, *38*, 400–404. [[CrossRef](#)]
37. Cagran, C.; Pottlacher, G. Normal spectral emissivities of liquid copper, liquid gold and liquid silver at 684.5 nm. *J. Non-Cryst. Solids* **2007**, *353*, 3582–3586. [[CrossRef](#)]
38. Kurosawa, R.; Inoue, T.; Baba, Y.; Sugioka, K.-I.; Kubo, M.; Tsukada, T.; Fukuyama, H. Normal spectral emissivity measurement of molten copper using an electromagnetic levitator superimposed with a static magnetic field. *Meas. Sci. Technol.* **2013**, *24*, 015603. [[CrossRef](#)]
39. Moores, A.; Goettmann, F. The plasmon band in noble metal nanoparticles: An introduction to theory and applications. *New J. Chem.* **2006**, *30*, 1121–1132. [[CrossRef](#)]
40. Kim, M.; Lee, J.-H.; Nam, J.-M. Plasmonic photothermal nanoparticles for biomedical applications. *Adv. Sci.* **2019**, *6*, 1900471. [[CrossRef](#)]
41. Gutiérrez, Y.; Brown, A.S.; Moreno, F.; Losurdo, M. Plasmonic beyond noble metals: Exploiting phase and compositional changes for manipulating plasmonic performance. *J. Appl. Phys.* **2020**, *128*, 080901. [[CrossRef](#)]
42. Sattler, K.D. (Ed.) *21st Century Nanoscience: A Handbook (Ten-Volume Set)*; CRC Press: New York, NY, USA, 2020.
43. Chan, G.H.; Zhao, J.; Hicks, E.M.; Schatz, G.C.; Van Duyne, R.P. Plasmonic properties of copper nanoparticles fabricated by nanosphere lithography. *Nano Lett.* **2007**, *7*, 1947–1952. [[CrossRef](#)]
44. Tien, C.L.; Drolen, B.L. Thermal radiation in particulate media with dependent and independent scattering. In *Annual Review of Numerical Fluid Mechanics and Heat Transfer*; Hemisphere: New York, NY, USA, 1987; Volume 1, pp. 1–32.
45. Ivezić, Ž.; Mengüç, M.P. An investigation of dependent/independent scattering regimes using a discrete dipole approximation. *Int. J. Heat Mass Transf.* **1996**, *39*, 811–822. [[CrossRef](#)]
46. Mishchenko, M.I. *Electromagnetic Scattering by Particles and Particle Groups: An Introduction*; Cambridge University Press: New York, NY, USA, 2014.
47. Mishchenko, M.I. “Independent” and “dependent” scattering by particles in a multi-particle group. *OSA Continuum.* **2018**, *1*, 243–260. [[CrossRef](#)]
48. Galy, T.; Huang, D.; Pilon, L. Revisiting independent versus dependent scattering regimes in suspensions or aggregates of spherical particles. *J. Quant. Spectr. Radiat. Transf.* **2020**, *246*, 106924. [[CrossRef](#)]

49. Liu, B.; Zhao, J.; Liu, L. Continuum approach based on radiation distribution function for radiative transfer in densely packed particulate system. *J. Quant. Spectr. Radiat. Transf.* **2020**, *253*, 107028. [[CrossRef](#)]
50. Dombrovsky, L.A.; Reviznikov, D.L.; Kryukov, A.P.; Levashov, V.Y. Self-generated clouds of micron-sized particles as a promising way of a solar probe shielding from intense thermal radiation of the Sun. *J. Quant. Spectr. Radiat. Transf.* **2017**, *200*, 234–243. [[CrossRef](#)]
51. Dombrovsky, L.A.; Zaichik, L.I. An effect of turbulent clustering on scattering of microwave radiation by small particles in the atmosphere. *J. Quant. Spectr. Radiat. Transf.* **2010**, *111*, 234–242. [[CrossRef](#)]
52. Fedorets, A.A.; Dombrovsky, L.A. Generation of levitating droplet clusters above the locally heated water surface: A thermal analysis of modified installation. *Int. J. Heat Mass Transf.* **2017**, *104*, 1268–1274. [[CrossRef](#)]
53. Fedorets, A.A.; Frenkel, M.; Shulzinger, E.; Dombrovsky, L.A.; Bormashenko, E.; Nosonovsky, M. Self-assembled levitating clusters of water droplets: Pattern-formation and stability. *Sci. Rep.* **2017**, *7*, 1888. [[CrossRef](#)]
54. Maxwell-Garnett, J.C. Colours in metal glasses and in metallic films. *Phil. Trans. R. Soc. Lond. A* **1904**, *203*, 385–420.
55. Choi, T.C. *Effective Medium Theory: Principles and Applications*; Oxford University Press: New York, NY, USA, 1999.
56. Dombrovsky, L.A.; Kokhanovsky, A.A. Light absorption by polluted snow cover: Internal versus external mixture of soot. *J. Quant. Spectr. Radiat. Transf.* **2020**, *242C*, 106799. [[CrossRef](#)]
57. Koledintseva, M.Y.; DuBroff, R.E.; Schwartz, R.W. Maxwell Garnett rule for dielectric mixtures with statistically distributed orientations of inclusions. *Prog. Electromag. Res.* **2009**, *99*, 131–148. [[CrossRef](#)]
58. Markel, V.A. Introduction to the Maxwell Garnett approximation: Tutorial. *J. Opt. Soc. Am. A* **2016**, *33*, 1244–1256. [[CrossRef](#)]
59. Born, M.; Wolf, E. *Principles of Optics*, 7th ed.; Cambridge University Press: Cambridge, UK, 2020.
60. Fedorets, A.A.; Frenkel, M.; Bormashenko, E.; Nosonovsky, M. Small levitating droplet clusters: Stability, symmetry, and Voronoi entropy. *J. Phys. Chem. Lett.* **2017**, *8*, 5599–5602. [[CrossRef](#)]